

A, with measurement errors below 1 dB for OSNR values below 32 dB. This validates the proposed monitoring method, even in conditions of significant signal distortion.

4. CONCLUSION

A novel OSNR monitoring method using an AH has been proposed and validated experimentally. This method consists in using a previous calibration that produces an RAH, obtained in conditions of low optical noise, in order to obtain the AH that would be expected in conditions of optical noise-induced degradation. Measurement errors below 1 dB have been verified for OSNR values below 32 dB. The proposed method shows resilience to GVD-induced distortion, maintaining the same 1-dB error margins verified without signal distortion. The principal limitation of the proposed method is a minimum average optical power required at the input of the monitoring device. In the case of the tested system, a minimum input power of -7.5 dBm was verified. It is shown that electrical bandwidth limitations may be required to reduce this value. This indicates that a compromise between minimum input power and maximum evaluated bit rate must be found.

Future work will involve monitoring of interferometric crosstalk and chromatic dispersion using derivatives of the proposed technique.

ACKNOWLEDGMENTS

The authors would like to thank Fernando Jesus and Daniel Fonseca for support in the experimental work and valuable comments, respectively.

REFERENCES

1. N. Hanik, A. Gladisch, C. Caspar, and B. Strelbel, Application of amplitude histograms to monitor performance of optical channels, *Electron Lett* 35 (1999), 403–404.
2. A. Teixeira, P. Andre, M. Lima, J. da Rocha, and J. Pinto, Characterization of high bit rate optical signals by low rate asynchronous sampling, *Proc LEOS 2002*, Glasgow, Scotland, 2002, paper ThA2.
3. M. Rasztovits-Wiech, K. Studer, and W. Leeb, Bit error probability estimation algorithm for signal supervision in all-optical networks, *Electron Lett* 35 (1999), 1754–1755.
4. I. Shake and H. Takara, Averaged Q -factor method using amplitude histogram evaluation for transparent monitoring of optical signal-to-noise ratio degradation in optical transmission system, *J Lightwave Technol* 20 (2002), 1367–1373.
5. G. Agrawal, *Fiber-optic communication systems*, 2nd ed., Wiley-Interscience, New York, 1997.

© 2006 Wiley Periodicals, Inc.

A METHOD TO SIMULTANEOUSLY EXTRACT THE SMALL-SIGNAL EQUIVALENT CIRCUIT AND NOISE PARAMETERS OF HETEROJUNCTION BIPOLAR TRANSISTORS

Ma. Carmen Maya, Antonio Lázaro, and Lluís Pradell
CICESE División de Física Aplicada
Departamento de Electrónica y Telecomunicaciones
Ensenada, B.C. México 22860

Received 3 January 2006

ABSTRACT: A method to extract the elements of the small-signal equivalent circuit and the noise parameters (NPs) of heterojunction bi-

polar transistors (HBTs) is presented. The extraction is done by simultaneous fitting of the measured S -parameters, noise figure (for a well-matched impedance), and NPs (estimated using the so-called F_{50} method). An additional error term, given by the root square sum of the differences between the NPs estimated from the F_{50} method and the NPs directly computed using the Hawkins model, is considered in order to avoid nonphysical results in the extraction of the intrinsic noise sources. To obtain the initial values of the equivalent-circuit elements, analytical expressions are applied under a number of bias conditions, namely, reverse bias, forward bias, and active bias. Experimental verification of the extraction of the equivalent-circuit elements and NPs of an HBT, up to 8 GHz, are presented, and the NPs are compared to those measured with an independent (tuner-based) method. The behavior of F_{min} extracted using the proposed method, as a function of the HBT collector current, is also presented. © 2006 Wiley Periodicals, Inc. *Microwave Opt Technol Lett* 48: 1372–1379, 2006; Published online in Wiley InterScience (www.interscience.wiley.com). DOI 10.1002/mop.21649

Key words: heterojunction bipolar transistor (HBT); small-signal model; noise model; noise parameters extraction

1. INTRODUCTION

Heterojunction bipolar transistors (HBTs) have demonstrated good low-noise performance in microwave frequencies, making them viable candidates for low-noise amplifier (LNA) applications [1, 2]. To guarantee the successful design of an HBT LNA, accurate characterizations of the device small-signal model and noise model are required.

Several methods have been proposed to extract the elements of the small-signal model of HBTs (see Fig. 1). Those can be divided into two groups: optimization-based methods and direct-extraction methods. The former obtain all or some of the elements using optimization algorithms. Some of them propose complex algorithms to avoid local minima [3, 4], or consider additional measurements to fit the response of some elements [5–7]. A problem with these optimization techniques is their dependence on the starting values, which may result in nonunique solutions for the extraction results. On the other hand, direct-extraction methods obtain involved analytical expressions of the Z -, Y -, or H -parameters of the small-signal equivalent circuit under a number of bias conditions, such as reverse bias, forward bias, and active bias [8–11]. To extract the values of the small-signal equivalent-circuit elements, the direct-extraction methods either consider some approximations at different frequency ranges [12, 13], or use addi-

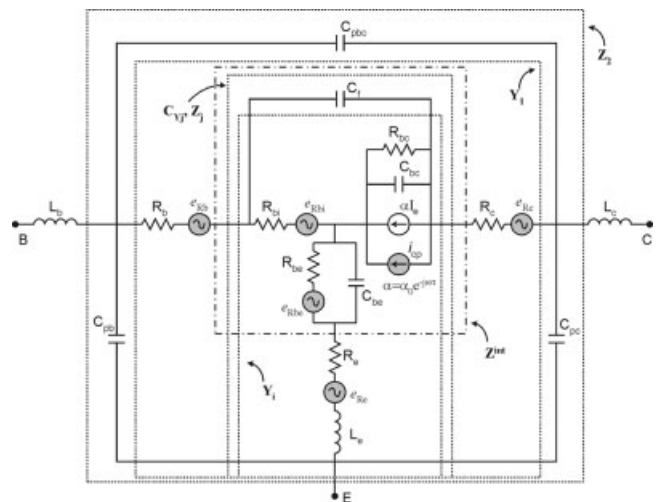


Figure 1 HBT small-signal equivalent circuit, in T-topology, including shot- and thermal-noise sources

tional structures to determine the values of the parasitic-element parameters [14]. The advantage of the direct-extraction methods (despite their complexity) is to provide physically significant values for the equivalent circuit parameters. Other methods combine both approaches by dividing the equivalent-circuit elements into two groups: extrinsic (or parasitic) and intrinsic elements. The extrinsic elements are obtained by optimization, whereas the intrinsic elements are determined by means of analytical expressions [15]; conversely, the extrinsic elements can also be obtained from measurements under reverse-bias and forward-bias conditions and the intrinsic elements are estimated by optimization [16].

The HBT noise behavior is described by its noise parameters (NPs). Several works in the literature propose models to compute the NPs of an HBT from the admittance parameters, [17–19], but those models only describe the intrinsic-device noise behavior. Additionally, the method in [18] requires previous knowledge of the values of the base and emitter resistances. Therefore, to use those models for obtaining the NPs, the parasitic elements must be extracted first from S -parameter or Y -parameter measurements, through a de-embedding procedure. In the work of Hawkins [20], the HBT noise model, and its noise parameters, can be obtained using the Hawkins model for the intrinsic noise sources, taking into account the extrinsic noise contributions. The Hawkins model assumes that the HBT intrinsic noise-sources are functions of the intrinsic resistances and the base transport factor, and that the extrinsic elements contribute only to thermal noise; hence, they can be directly computed from the small-signal circuit elements [21]. However, measurement uncertainties, local minima of the error function to be minimized (in optimization methods), and the approximations (assumed in the direct-extraction methods) will compromise the accuracy of the small-signal circuit elements' extraction, thus producing a misleading estimation of the noise sources, and therefore the four NPs, that is, minimum noise figure F_{min} , equivalent noise resistance R_n , and magnitude $|\Gamma_{opt}|$ and phase ϕ_{opt} of the optimum source reflection coefficient Γ_{opt} . To overcome this drawback, other works [22, 23] have proposed fitting the S -parameters and the NPs simultaneously. However, the measurement of NPs in [22, 23] requires an input tuner [24] to synthesize the multiple source impedances required at the HBT input (base) port (typically, 10 source states or more at each frequency). In [25] an intrinsic noise model (admittance noise-matrix configuration) was proposed to extract the NPs using new analytical expressions; however, the accuracy of the method still depends on the extraction quality of the small-signal parameters. Recently, a method to extract the NPs by fitting measurements and estimations of the noise figure has been proposed [26]. The analytical expressions presented in [25] were used to obtain the initial values, which are function of the small-signal model parameters and are also obtained through an optimization procedure.

In this paper, we propose a new method to simultaneously extract both the small-signal and noise model of the HBT using only measurements of the S -parameters and noise figures. Hence, a tuner to measure the NPs of the HBT is no longer required, which reduces the time, complexity, and cost of the measurements. Specifically, instead of measuring the NPs, the so-called F_{50} method [27] is used to extract the HBT intrinsic noise-sources. The F_{50} method, based on measuring the device noise figure as a function of frequency for a well-matched source impedance (therefore, only one source state per frequency is required), was previously applied to determine the four NPs of FETs without using tuner [27]. This method uses frequency redundancy rather than source-state redundancy (as in the tuner-based methods), assuming a smooth frequency dependence for the elements of the intrinsic-noise correlation matrix, which can be interpolated in frequency with a low-order polynomial. Therefore, we develop an optimization method to extract the small-equivalent equivalent-circuit elements,

with the noise model as a function of these elements [28]. The error function to be minimized in the optimization process is the sum of three terms, the root sum of squares (RSS) of the differences between the measured and estimated S -parameters, the RSS of the differences between measured and estimated noise figure (from the Hawkins model [20, 21]), and an additional term given by the RSS of the differences between the NPs obtained from the F_{50} method and those NPs estimated from the Hawkins model. This last term helps to avoid local minima, which would produce nonphysical NPs results. To obtain the initial values, analytical expressions are determined at different bias conditions applying some frequency approximations, as in [12, 16]. The procedure to compute the initial values is described in section 2, the noise-model extraction using the F_{50} method is developed in section 3, the minimization procedure is explained in section 4, and the experimental results of the small-signal and noise-model of a GaAs HBT, extracted up to 8 GHz, are presented in section 5.

2. SMALL-SIGNAL MODEL

The HBT small-signal equivalent circuit, in T-topology, is shown in Figure 1, where the intrinsic and the parasitic device noise-sources are included. The elements of the equivalent circuit are split into extrinsic (parasitic) and intrinsic elements. The former are assumed bias-independent and obtained by applying approximations at low frequency under reverse-bias and forward-bias conditions, as in [16]. Specifically, the parasitic capacitances C_{pb} , C_{pe} , and C_{pbc} are extracted from the Y -parameter measurements of the device under reverse-bias condition ($V_{be} < 0$ V and $V_{ce} = 0$ V), for which the simplified equivalent circuit shown in Figure 2(a) holds. Under these conditions, the admittance parameters have a linear frequency dependence and are basically capacitive in the lower-frequency range. The extrinsic resistances R_b , R_c , and R_e and the inductances L_b , L_c , and L_e are computed from the Z -parameter measurements of the device under forward-bias condition ($V_{be} > 0$ V and $V_{ce} = 0$ V), for which the simplified equivalent circuit shown in Figure 3(a) holds. Under forward-bias conditions, the real part of the device impedance is basically constant with frequency and the imaginary part has an inductive linear frequency dependence. Figures 2 and 3 illustrate the behavior of the measured admittance and impedance parameters of a GaAs HBT ($2 \times 320 \mu\text{m}^2$ emitter area) under forward bias and reverse bias, respectively. In Figures 3(b) and 3(c), it is observed that, under forward-bias conditions, the effects of the intrinsic elements are still present, since the imaginary part of the impedance Z_{12} is negative, and the real part is constant only at high frequencies. This effect is due to the influence of a distributed diode between the base and the collector and between the base and the emitter. Hence, we propose to use the measurements under reverse [Fig. 2(b)] and forward [Figs. 3(b) and 3(c)] conditions to compute an initial estimation of the extrinsic elements. These values are introduced in an optimization algorithm in order to minimize an error function, as explained in section 4.

The intrinsic elements depend on the device bias. They are obtained by fitting the estimated and the measured S -parameters under active-bias conditions. The initial values are computed using the following procedure.

First, the extrinsic elements are de-embedded, from the measured S -parameters, in order to determine the intrinsic impedance matrix, \mathbf{Z}^{int} (Fig. 1). Then, the following relations of the elements of \mathbf{Z}^{int} [12], are used to estimate the values of the intrinsic elements:

$$Z_{11}^{\text{int}} - Z_{12}^{\text{int}} = \frac{R_{bi}Z_f}{R_{bi} + Z_f + Z_{bc}} = \frac{R_{bi} + j\omega R_{bi}R_{bc}C_{bc}}{D},$$

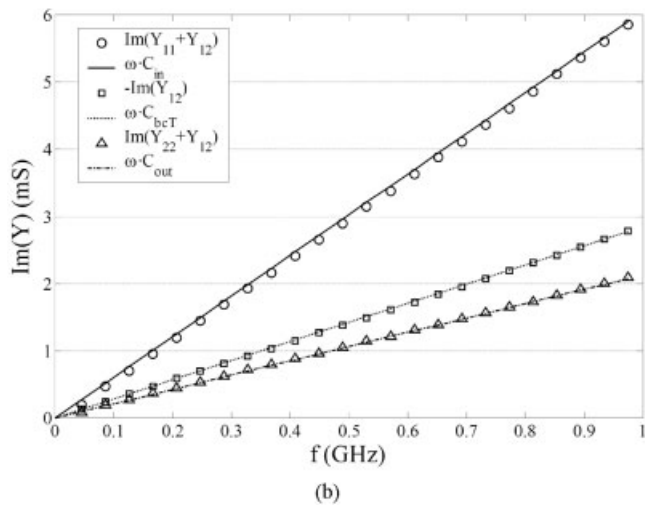
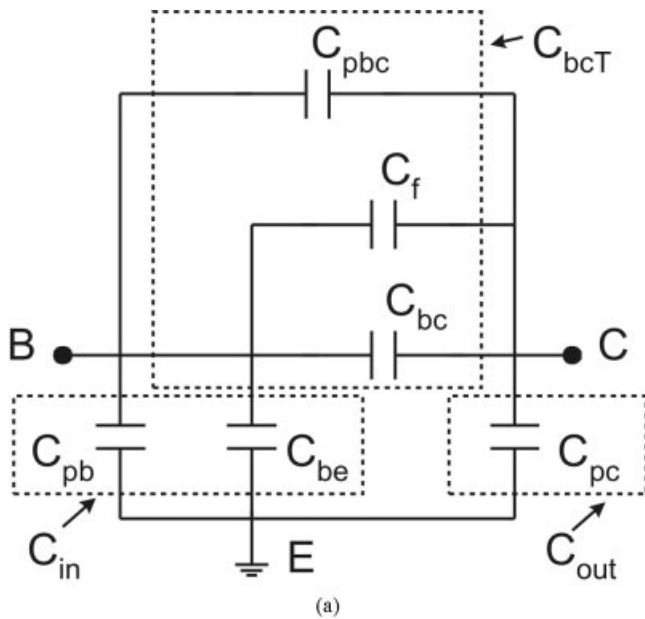


Figure 2 (a) HBT equivalent circuit under reverse bias ($C_{in} = C_{pb} + C_{be}$, $C_{bcT} = C_{pbc} + C_f + C_{bc}$, and $C_{out} = C_{pc}$), (b) imaginary part of the admittance parameters $[Y]$ of a GaAs HBT with $V_{ce} = 0$ V and $V_{be} = -2.0$ V

$$Z_{22}^{int} - Z_{21}^{int} = \frac{Z_f Z_{bc}}{R_{bi} + Z_f + Z_{bc}} = \frac{R_{bc}}{D},$$

$$Z_{12}^{int} - Z_{21}^{int} = \frac{\alpha Z_f Z_{bc}}{R_{bi} + Z_f + Z_{bc}} = \frac{\alpha R_{bc}}{D},$$

$$D = 1 - \omega^2 R_{bi} R_{bc} C_{bc} C_f + j\omega [R_{bc}(C_{bc} + C_f) + R_{bi} C_f], \quad (1)$$

with

$$Z_f = 1/(j\omega C_f),$$

$$Z_{bc} = R_{bc} / (1 + j\omega C_{bc} R_{bc}),$$

$$Z_{be} = R_{be} / (1 + j\omega C_{be} R_{be}). \quad (2)$$

The base transport factor, α , is directly computed from [21]:

$$\alpha = \alpha_0 e^{-j\omega\tau} = \frac{Z_{12}^{int} - Z_{21}^{int}}{Z_{22}^{int} - Z_{21}^{int}}, \quad (3)$$

where α_0 the magnitude of α , $-j\omega\tau$ its phase and τ is the transit time. When $\omega \rightarrow 0$, the intrinsic base resistance can be approximated by

$$R_{bi} \approx \text{Re}(Z_{11}^{int} - Z_{12}^{int}) \quad (4)$$

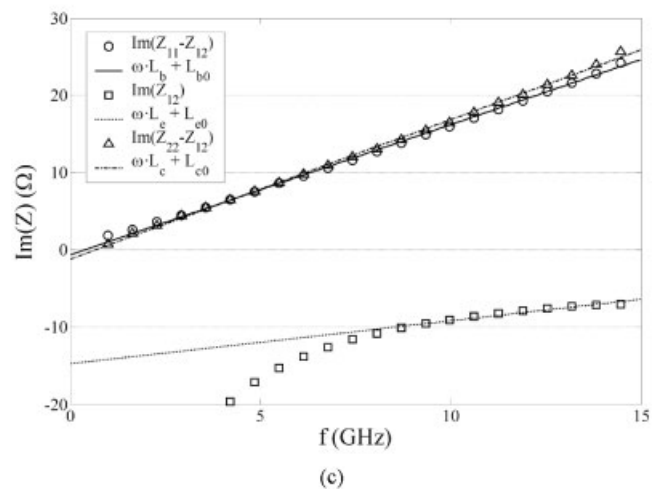
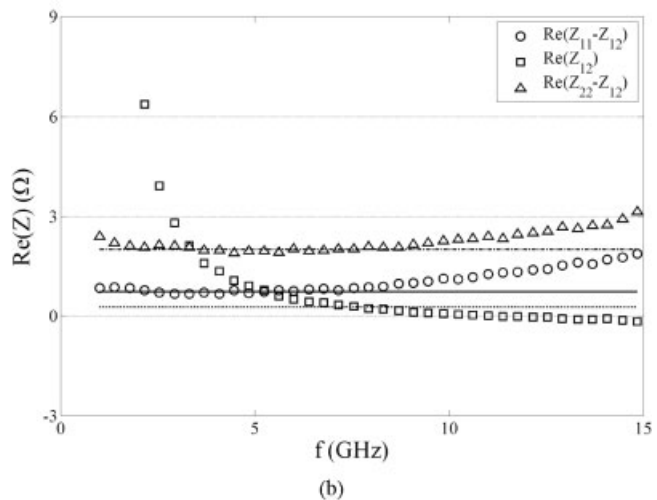
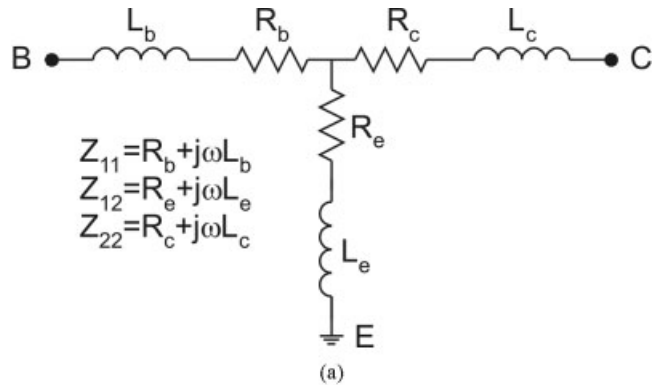


Figure 3 (a) HBT equivalent circuit under forward bias; (b) real part and (c) imaginary part of the impedance parameters $[Z]$ of a GaAs HBT with $V_{ce} = 0$ V and $V_{be} = 1.2$ V (L_{b0} , L_{e0} , and L_{c0} are the independent terms of the imaginary part of the Z -parameters)

and the base-collector resistance by

$$R_{bc} \approx \operatorname{Re} \left(\frac{Z_{22}^{\text{int}} - Z_{21}^{\text{int}}}{Z_{11}^{\text{int}} - Z_{12}^{\text{int}}} \right) R_{bi}. \quad (5)$$

The auxiliary variable D in (1) is computed as:

$$D = \frac{R_{bc}}{Z_{22}^{\text{int}} - Z_{21}^{\text{int}}}. \quad (6)$$

Then, the base-collector capacitance is determined as

$$C_{bc} = \frac{\operatorname{Im}(D \cdot (Z_{11}^{\text{int}} - Z_{12}^{\text{int}}))}{\omega R_{bc} R_{bi}} \quad (7)$$

and the feedback capacitance C_f as

$$C_f = \frac{\frac{\operatorname{Im}(D)}{\omega} - R_{bc} C_{bc}}{R_{bc} + R_{bi}}. \quad (8)$$

The equivalent impedance of the base-emitter branch is defined as

$$Z_{be} = \frac{R_{be} - j\omega R_{be}^2 C_{be}}{1 + (\omega R_{be} C_{be})^2} = Z_{12}^{\text{int}} - \frac{(1 - \alpha)j\omega R_{bi} R_{bc} C_f}{D}. \quad (9)$$

If $(\omega R_{be} C_{be})^2 \ll 1$, then

$$R_{be} \approx \operatorname{Re}(Z_{be}), \quad (10)$$

$$C_{be} \approx -\frac{\operatorname{Im}(Z_{be})}{\omega R_{be}^2}. \quad (11)$$

As pointed out above, the final values of the intrinsic elements are computed by applying an optimization algorithm. The final values of the elements of the equivalent circuit are obtained using the procedure described in section 4, in which the device noise figure and NPs are also taken into account.

3. NOISE MODEL EXTRACTION

The Hawkins model [20] is used to describe the intrinsic transistor noise, where two uncorrelated shot noise sources i_{cp} and $e_{R_{be}}$, whose mean quadratic values are functions of the intrinsic base-emitter resistance R_{be} and the base transport factor α , are considered (Fig. 1):

$$\overline{i_{cp}^2} = \frac{2kT_a(\alpha_0 - |\alpha|^2)}{R_{be}} \Delta f, \quad (12)$$

$$\overline{e_{R_{be}}^2} = 2kT_a R_{be} \Delta f, \quad (13)$$

where α_0 is the low-frequency value of α , Δf is the noise integration bandwidth, T_a is the room temperature, and k is the Boltzmann's constant. Also, a thermal noise contribution from resistance R_{bi} is assumed, whose mean quadratic value is given by

$$\overline{e_{R_{bc}}^2} = 4kT_a R_{bi} \Delta f. \quad (14)$$

In the same way, it is assumed that the parasitic resistances (R_b , R_c , and R_e) have a thermal noise contribution:

$$\overline{e_{R_x}^2} = 4kT_a R_x \Delta f, \quad (15)$$

where $x = b, c, e$, respectively. The NPs are computed from the total noise-correlation matrix in its cascade representation (\mathbf{C}_{AT}) of the HBT equivalent circuit [29]. The matrix \mathbf{C}_{AT} results from the following noise analysis, in which it is expressed as a function of the intrinsic and extrinsic noise contributions:

$$\mathbf{C}_{\text{AT}} = \mathbf{P}_2 \cdot \mathbf{C}_{\text{Y}_j} \cdot \mathbf{P}_2^\dagger + \mathbf{C}_{\text{A}}^{\text{ext}}, \quad (16)$$

where

$$\mathbf{C}_{\text{Y}_j} = \mathbf{Y}_j \cdot \begin{bmatrix} \overline{e_1^2} & \overline{e_1 e_2^*} \\ \overline{e_2 e_1^*} & \overline{e_2^2} \end{bmatrix} \cdot (\mathbf{Y}_j)^\dagger, \quad (17)$$

$$\overline{e_1^2} = \overline{e_{R_e}^2} + 4kT_a R_{bi} + |Z_{be}|^2 \frac{\overline{e_{R_{be}}^2}}{R_{be}^2},$$

$$\overline{e_2^2} = \overline{e_{R_e}^2} + |Z_{bc}|^2 i_{cp}^2 + |Z_{be}|^2 \frac{\overline{e_{R_{be}}^2}}{R_{be}^2},$$

$$\overline{e_1 e_2^*} = \overline{e_2 e_1^*} = \overline{e_{R_e}^2} + |Z_{be}|^2 \frac{\overline{e_{R_{be}}^2}}{R_{be}^2}, \quad (18)$$

$$\mathbf{C}_{\text{A}}^{\text{ext}} = \mathbf{P}_1 \cdot \begin{bmatrix} \overline{e_{R_b}^2} & 0 \\ 0 & \overline{e_{R_c}^2} \end{bmatrix} \cdot \mathbf{P}_1^\dagger, \quad (19)$$

$$\mathbf{P}_1 = \begin{bmatrix} 1 & -A_{T11} \\ 0 & -A_{T21} \end{bmatrix} \cdot \mathbf{Z}_2 \cdot \mathbf{Y}_j; \quad \mathbf{P}_2 = \mathbf{P}_1 \cdot \mathbf{Z}_j. \quad (20)$$

In (16)–(20), the superscript ‘ \dagger ’ denotes the transpose-conjugated operator, \mathbf{Y}_j is the admittance matrix of the intrinsic part (without including the feedback capacitance C_f) adding the emitter resistance R_e and inductance L_e , \mathbf{Z}_j is the impedance matrix of the former block (\mathbf{Y}_j) in parallel with C_f , \mathbf{Y}_1 is the admittance matrix corresponding to block \mathbf{Z}_j in series with the resistances R_b and R_c , and \mathbf{Z}_2 is the impedance matrix of the device, without considering the extrinsic base and collector inductances, L_b and L_c , respectively (see Fig. 1). Matrix $\mathbf{C}_{\text{A}}^{\text{ext}}$ groups the extrinsic contributions, whereas the first term of the right-hand side of (16) includes the intrinsic contribution (\mathbf{C}_{Y_j}) as well as the emitter-resistance contribution.

Note that the direct-extraction method proposed here can be directly applied to Π -configuration of the small-signal equivalent circuit or Y representation. In this case, the admittance correlation matrix (17) is obtained from base and collector noise sources (base and collector shot noise and the correlation between the noise sources due to the transit time [30, 31]).

From (12)–(20), it is observed that the NPs can be easily calculated, if the equivalent circuit elements are known, using the expressions for the NPs of a two-port as a function of its \mathbf{C}_{AT} presented in [29].

To extract the elements of the intrinsic-noise correlation matrix \mathbf{C}_{Y_j} , we propose to use the F_{50} method, similarly to [27] for FETs. Using the definition of the noise figure as a function of the source impedance Z_s and of the device noise correlation matrix \mathbf{C}_{AT} given in (16) [28, 29]:

$$F_{\text{TRT}}(Z_s^i) = 1 + \frac{(\mathbf{Z}^i) \cdot \mathbf{C}_{\text{AT}} \cdot (\mathbf{Z}^i)^\dagger}{4kT_0 \operatorname{Re}(Z_s^i)}, \quad \mathbf{Z}^i = [1 \ (Z_s^i)^*], \quad (21)$$

where $T_0 = 290^\circ\text{K}$ is the standard temperature, and $\mathbf{Z}_s^i = R_s^i + jX_s^i$ is the source impedance measured at the i^{th} frequency point. Usually, the source impedance Z_s is either well-matched (50Ω)—thus F_{TRT} is called F_{50} —or near 50Ω , in order to avoid transistor oscillations. Then, substituting (16) into (21), the intrinsic contribution is expressed in terms of the noise figure (measured at N_f frequency points) and $\mathbf{C}_A^{\text{ext}}$ as follows:

$$(\mathbf{Z}^i \cdot \mathbf{P}_2) \cdot \mathbf{C}_{Y_j} \cdot (\mathbf{Z}^i \cdot \mathbf{P}_2)^\dagger = 4kT_0 \text{Re}(\mathbf{Z}_s^i) \cdot [F_{TRT}(\mathbf{Z}_s^i) - 1] - (\mathbf{Z}^i) \cdot \mathbf{C}_A^{\text{ext}} \cdot (\mathbf{Z}^i)^\dagger. \quad (22)$$

Reordering (22) and making a change of variable, the following linear equation system for the i^{th} frequency point is obtained for \mathbf{C}_{Y_j} :

$$\Delta^i = [M_1^i \ M_2^i \ M_3^i \ M_4^i] \cdot [C_{Y_{j11}} \ C_{Y_{j22}} \ \text{Re}(C_{Y_{j12}}) \ \text{Im}(C_{Y_{j12}})]^T, \quad (23)$$

$$M_1^i = |P_{2,11}|^2 + |Z_s^i|^2 |P_{2,21}|^2 + 2R_s^i \text{Re}(P_{2,11} P_{2,21}^*) - 2X_s^i \text{Im}(P_{2,11} P_{2,21}^*),$$

$$M_2^i = |P_{2,12}|^2 + |Z_s^i|^2 |P_{2,22}|^2 + 2R_s^i \text{Re}(P_{2,12} P_{2,22}^*) - 2X_s^i \text{Im}(P_{2,12} P_{2,22}^*),$$

$$M_3^i = 2 \text{Re}(P_{2,11} P_{2,12}^*) + 2|Z_s^i|^2 \text{Re}(P_{2,21} P_{2,22}^*) + 2R_s^i \text{Re}(P_{2,11} P_{2,22}^* + P_{2,12} P_{2,21}^*) - 2X_s^i \text{Im}(P_{2,11} P_{2,22}^* + P_{2,12} P_{2,21}^*),$$

$$M_4^i = 2 \text{Im}(P_{2,11} P_{2,12}^*) - 2|Z_s^i|^2 \text{Im}(P_{2,21} P_{2,22}^*) - 2R_s^i \text{Im}(P_{2,11} P_{2,22}^* - P_{2,12} P_{2,21}^*) - 2X_s^i \text{Re}(P_{2,11} P_{2,22}^* - P_{2,12} P_{2,21}^*), \quad (24)$$

$$\Delta^i = 4kT_0 \text{Re}(\mathbf{Z}_s^i) \cdot [F_{TRT}(\mathbf{Z}_s^i) - 1] - (\mathbf{Z}^i) \cdot \mathbf{C}_A^{\text{ext}} \cdot (\mathbf{Z}^i)^\dagger. \quad (25)$$

In (23), the superscript T denotes the transpose operator and the unknown correlation matrix \mathbf{C}_{Y_j} has been arranged as a column vector whose elements are $C_{Y_{j11}}$, $C_{Y_{j22}}$, and the real and imaginary part of $C_{Y_{j12}}$, $\text{Re}(C_{Y_{j12}})$, and $\text{Im}(C_{Y_{j12}})$, respectively. If a redundant number of frequency points ($N_f > 4$) is considered, the expression (23) is an overdetermined linear equation system. This expression is similar to (5) in [27] for FET devices, where it is assumed that the four unknowns have a smooth frequency dependence that can be interpolated using an L -order polynomial; applying the same principle here each unknown can be expanded as:

$$C_{ij} = \sum_{l=0}^L f^l C_{ij}^l; \quad C_{ij} = C_{Y_{j11}}, C_{Y_{j22}}, \text{Re}(C_{Y_{j12}}), \text{ and } \text{Im}(C_{Y_{j12}}). \quad (26)$$

In this work it is assumed that $L = 2$ for all the elements, except $\text{Im}(C_{Y_{j12}})$, for which $L = 1$ is considered. These figures for L are selected according to the frequency dependence of the power spectral densities observed in (18). Then, substituting (26) into (23), an equation system with eight unknowns (polynomial coefficients C_{ij}^l) is obtained. The unknowns are computed (estimated) using an optimization algorithm for the best fit of the computed F_{50} [(23)–(26)] to the measured noise figure. The initial values are computed using the pseudo-inverse method to (23); then, according to their decreasing sensitivity, each element is obtained according to the following optimization order: C_{22}^0 , C_{22}^1 , C_{22}^2 , C_{11}^0 , C_{11}^1 , C_{11}^2 , $\text{Re}(C_{12})^0$, $\text{Re}(C_{12})^1$, $\text{Re}(C_{12})^2$, $\text{Im}(C_{12})^0$,

and $\text{Im}(C_{12})^1$. The optimization limits are set in such a way that the elements of the correlation matrix meet the following conditions:

$$C_{Y_{j11}} \geq 0; \quad C_{Y_{j22}} \geq 0; \quad 0 \leq |\rho| = \left| \frac{C_{Y_{j12}}}{\sqrt{C_{Y_{j11}} \cdot C_{Y_{j22}}}} \right| \leq 1, \quad (27)$$

where ρ is the correlation coefficient of the intrinsic noise sources.

4. OPTIMIZATION ALGORITHM

As pointed out in section 2, the extracted equivalent-circuit elements must be consistent with the noise model [Hawkins model, see (12)–(20)]. To this end, an optimization method is applied, where an error function is minimized. The error function is defined as the weighted-sum of individual errors, initially e_S and e_{NF} , defined as the RSS of the difference between the measured and the estimated S -parameters:

$$e_S = \frac{1}{N_f} \sqrt{\sum_{j=1}^4 \sum_{i=1}^{N_f} (S_{jm}^i - S_{je}^i)^2} \quad (28)$$

and as the RSS of the difference between the measured noise figure (NF_m) and noise figure estimated from the Hawkins' model (NF_e):

$$e_{NF} = \frac{1}{N_f} \sqrt{\sum_{i=1}^{N_f} (NF_m^i - NF_e^i)^2}. \quad (29)$$

In (28) and (29), the subscript j denotes the four S -parameters ($j = 11, 12, 21, 22$), m denotes measures and e denotes estimated values. However, it is observed that if the optimization method only minimizes the errors of the S -parameters and noise figure (e_S and e_{NF}), the results of the NPs may be misleading in spite of the good agreement between the estimated noise figure and the measurements, since the optimization method converges to a local minimum. To avoid this drawback, the F_{50} method described in section 3 is used to extract the noise correlation-matrix \mathbf{C}_{Y_j} of the intrinsic part plus the resistance R_e and the inductance L_e (see Fig. 1). Then, the contributions of the base and collector resistors are added and finally the NPs are computed from the expressions of the total cascade noise correlation matrix. Note that, to use the F_{50} method, only the extrinsic elements must be known, since the matrices \mathbf{Z}_j , \mathbf{Y}_1 , and \mathbf{Z}_2 (Fig. 1) are determined by subtracting the effect of those elements from the measured total impedance from those computed from the measured S -parameters. Thus, an additional error term, e_{NP} , is considered simultaneously with e_S and e_{NF} in the optimization algorithm, given by the RSS of the differences between the NPs estimated from the F_{50} method, NP_{F50} , and NPs directly computed using the Hawkins' model, NP_H :

$$e_{NP} = \frac{1}{N_f} \sqrt{\sum_{j=1}^4 \sum_{i=1}^{N_f} (NP_{H,j}^i - NP_{F50,j}^i)^2}. \quad (30)$$

In (30), the subscript j denotes one of the four NPs, F_{min} , R_n , $|\Gamma_{opt}|$, and Φ_{opr} . Then, the total error term to minimize is $e_T = w_1 e_S + w_2 e_{NF} + w_3 e_{NP}$, where w_1 , w_2 , and w_3 are weighting factors. The optimization procedure (see flowchart in Fig. 4) is as follows: (i) first, the initial values of the equivalent circuit elements are estimated by the procedure described in section 2, and the intrinsic elements are computed using (3)–(11); (ii)

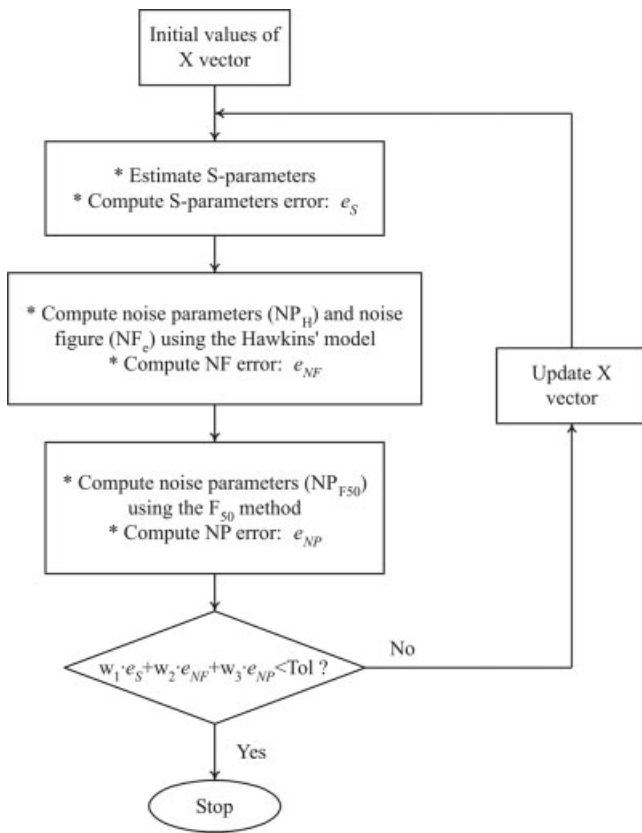


Figure 4 Flowchart to extract the elements of the small-signal equivalent circuit. $X = [C_{pb}, C_{pe}, C_{pbc}, L_b, L_c, L_e, R_b, R_c, R_e, R_{bc}, C_{bc}, R_{bi}, C_f, R_{be}, C_{be}, \alpha_0, \tau]$; w_1, w_2 , and w_3 are the weighting factors of the error function e_T

next, e_S is evaluated using (28); (iii) the noise parameters NP_H and noise figure NF_e are estimated using the Hawkins model [(12)–(20)], and e_{NF} is evaluated using (29); (iv) the NPs are estimated by applying the F_{50} method (NP_{F50}) with (23)–(26), and e_{NP} is evaluated using (30); (v) finally, the total error e_T is evaluated and compared to a predefined tolerance value (Tol). If e_T is larger than Tol , the elements of the equivalent circuit are

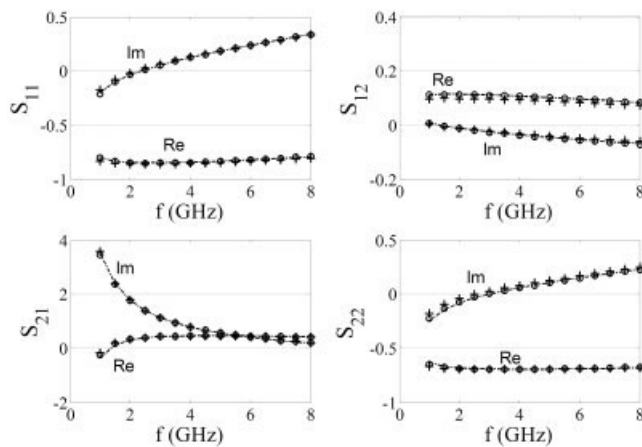


Figure 5 Real and imaginary part of the GaAs HBT S -parameters: measured (\circ) and estimated by minimization of e_S ($-\triangle-$) and by applying the proposed method (minimization of e_T) ($+$). Bias points: $V_{ce} = 0.5$ V and $I_{ce} = 11.2$ mA

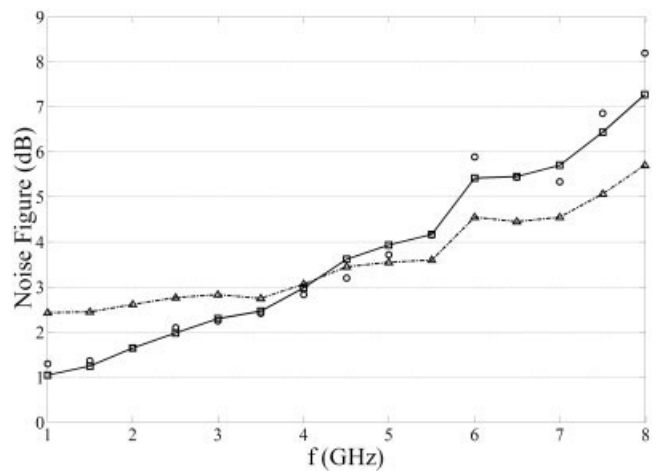


Figure 6 GaAs HBT noise figure: measured (\circ) and estimated from the elements of the equivalent circuit extracted by minimization of e_S ($-\triangle-$) and by applying the proposed method (minimization of e_T) ($-\square-$). Bias point: $V_{ce} = 0.5$ V and $I_{ce} = 11.2$ mA

updated and the process is repeated from step ii until the error reaches the Tol .

5. RESULTS

The proposed method has been used to characterize a GaAs HBT with $2 \times 320 \mu\text{m}^2$ emitter area, biased at $V_{ce} = 0.5$ V and $I_{ce} = 11.2$ mA. The S -parameters, noise parameters, and noise figure were estimated using the elements of the equivalent circuit extracted by minimizing the e_S error only, and by applying the procedure proposed in this work (minimizing e_T to simultaneously fit the S -parameters, noise-figure measurements, and NPs). Figure 5 compares the S -parameter measurements with the estimations from minimization of e_S only, and minimizing e_T , good agreement is shown in both cases. Figure 6 shows the noise-figure measurements of the device, compared with the estimations by minimizing e_S only and minimizing e_T (the proposed method), respectively. It can be observed that, although the S -parameters fit correctly when minimizing e_S only (see Fig. 5), the estimated noise figure does not match the measured noise figure, whereas if e_T is minimized, both the estimated S -parameters and the estimated noise figure are in agreement with the measurements.

Figure 7 shows the estimations of the noise parameters from minimization of e_S only and minimizing e_T , respectively. As a consequence of the disagreement of the noise-figure results when only the S -parameters are optimized, the estimated NPs may be spurious. This is observed mainly in the minimum noise figure F_{min} , which presents a small negative slope, whereas the results from the proposed method show an increase with frequency, thus agreeing with the results in the literature [21, 32]. The three other NPs show a similar frequency response in both cases. Table 1 gives the initial values of the equivalent circuit elements and the results from minimization of e_S and of e_T . It is observed that C_{pb} , L_e , C_{bc} , C_{be} , and R_{bc} are the elements showing the largest variation between the initial values and results from minimization of e_T . The variation in C_{pb} is due to the effect of the intrinsic part, which is still significant when the device is reverse-biased, due to the distributed diode between the base and the collector and between the base and the emitter [16]. A similar effect happens when L_e is estimated, whereas the variation of C_{bc} , C_{be} , and R_{bc} is a consequence of the deviations in the extrinsic values.

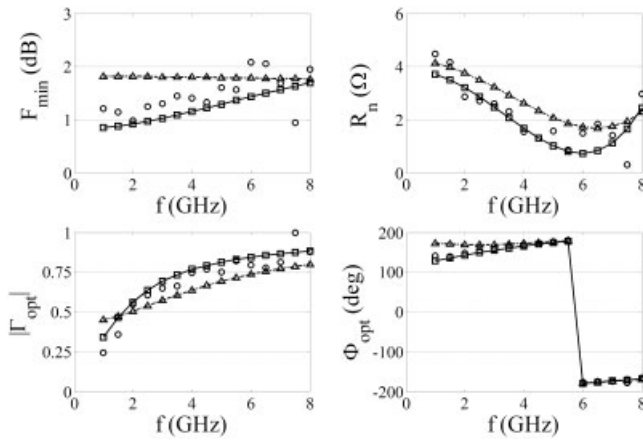


Figure 7 GaAs HBT noise parameters (F_{min} , R_n , and $\Gamma_{opt} = |\Gamma_{opt}|e^{j\Phi_{opt}}$) measured using a tuner-based method (\circ) and estimated from the elements of the equivalent circuit extracted by minimization of e_s (\triangle) and by applying the proposed method (minimization of e_r) (\square). Bias points: $V_{ce} = 0.5$ V and $I_{ce} = 11.2$ mA

To verify the results obtained for the NPs, a comparison with independent results is performed. Indeed, the NPs have been measured using a tuner-based method [24], which does not require an estimation of the equivalent circuit. The results are also plotted in Figure 7. Very good agreement is observed between the NPs measured using the tuner method and estimated using the method proposed herein.

Figure 8 plots F_{min} as a function of the collector current I_{ce} measured by applying the proposed method. It can be seen that F_{min} increases with I_{ce} , which agrees with the results reported in the literature for GaAs HBTs [21, 32], and SiGe HBTs [19]. This effect is mainly due to the contribution associated with the emitter-base resistance, which is inversely proportional to the collector current, and thus the shot-noise contribution becomes more important.

TABLE 1 Equivalent-Circuit Elements of the GaAs HBT Biased at $V_{ce} = 0.5$ V and $I_{ce} = 11.2$ mA

	Extrinsic Elements		
	Initial values	Minimizing e_s	Minimizing e_r
C_{pb} (pF)	0.60	0.68	1.48
C_{pc} (pF)	0.34	0.35	0.35
C_{pbc} (pF)	0.13	0.14	0.005
L_b (pH)	268.36	240.34	231.82
L_c (pH)	287.06	241.98	238.91
L_e (pH)	88.49	0.0035	5.78
R_b (Ω)	0.55	0.58	0.71
R_c (Ω)	1.35	1.29	1.78
R_e (Ω)	0.91	2.81	1.53
	Intrinsic Elements		
R_{bc} (k Ω)	0.74	1.48	1.89
C_{bc} (pF)	0.43	0.01	0.01
R_{bi} (Ω)	0.45	0.01	0.63
C_f (pF)	0.69	1.15	1.32
R_{be} (Ω)	2.88	1.01	1.70
C_{be} (pF)	11.45	2.64	0.01
α_0	0.98	0.98	0.99
τ (ps)	5.33	5.12	2.20

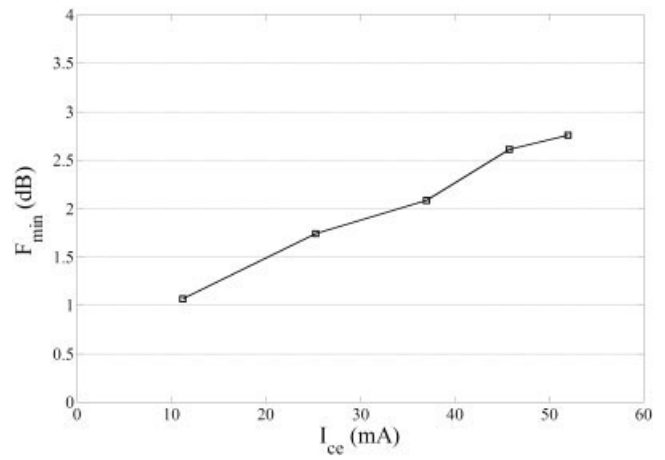


Figure 8 GaAs HBT minimum noise figure measured with the proposed method vs. the collector-emitter current I_{ce} at 3 GHz

6. CONCLUSION

A method for a reliable characterization of the small-signal equivalent circuit and the noise model of HBTs has been presented. It allows the device equivalent-circuit elements (in T-topology) and its noise parameters to be extracted simultaneously, using only the measurements of the device S -parameters and noise figure for a well-matched impedance. To avoid nonphysical results, the F_{50} method is used to generate an additional error term in the minimization procedure. Using the proposed method, the noise parameters of a GaAs HBT have been measured up to 8 GHz, exhibiting excellent agreement with the measurements using the tuner-based method.

ACKNOWLEDGMENT

The authors are indebted to Jorge Calvín and Joan Casas, from MIER Comunicaciones, S.A., Barcelona, for providing the HBT devices. This work has been partially supported by the Spanish Government Projects ESP2004-07067-C03-03 (Plan Nacional I + D + I) and TEC2005-06297/MIC, and a scholarship from CONACYT-Mexico.

REFERENCES

1. J. Lee, G. Lee, G. Niu, J.D. Cressler, J.H. Kim, J.C. Lee, B. Lee, and N.Y. Kim, The design of SiGe HBT LNA for IMT-2000 mobile application, IEEE MTT-S Dig (2002), 1261–1264.
2. K.W. Kobayashi, A.K. Oki, L.T. Tran, and D.C. Streit, Ultra-low dc power GaAs HBT S- and C-band low noise amplifiers for portable wireless applications, IEEE Trans Microwave Theory Tech 43 (1995), 3055–3061.
3. B. Meskoob, S. Prasad, M. Vai, C.G. Fonstad, J.C. Vlcek, H. Sato, and C. Bulutay, A small-signal equivalent circuit for the collector-up InGaAs/InAlAs/InP heterojunction bipolar transistor, IEEE Trans Electron Devices 39 (1992), 2629–2632.
4. R. Menozzi, M. Borgarino, J. Tasselli, and A. Marty, HBT small-signal model extraction using a genetic algorithm, IEEE MTT-S Dig (1998), 157–160.
5. B. Willén, M. Rohner, I. Schnyder, and H. Jäckel, Improved automatic parameter extraction of InP-HBT small-signal equivalent circuits, IEEE Trans Microwave Theory Tech 50 (2002), 580–583.
6. S. Lee, Fast and efficient extraction of HBT model parameters using

- multibias S-parameters sets, *IEEE Trans Microwave Theory Tech* 44 (1996), 1499–1502.
7. H. Ghaddab, F.M. Ghannouchi, F. Choubani, and A. Bouallegue, Small-signal modeling of HBT's using a hybrid optimization/statistical technique, *IEEE Trans Microwave Theory Tech* 46 (1998), 292–298.
 8. C.-J. Wei and J.C.M. Hwang, Direct extraction of equivalent circuit parameters for heterojunction bipolar transistors, *IEEE Trans Microwave Theory Tech* 43 (1995), 2035–2040.
 9. M. Sotoodeh, L. Sozzi, A. Vinay, A.H. Khalid, Z. Hu, A.A. Rezazadeh, and R. Menozzi, Stepping toward standard methods of small-signal parameter extraction for HBT's, *IEEE Trans Electron Device* 47 (2000), 1139–1151.
 10. M. Rudolph, R. Doerner, and P. Heymann, Direct extraction of HBT equivalent-circuit elements, *IEEE Trans Microwave Theory Tech* 47 (1999), 82–84.
 11. D.R. Pehlke and D. Pavlidis, Evaluation of the factors determining HBT high-frequency performance by direct analysis of S-parameter data, *IEEE Trans Microwave Theory Tech* 40 (1992), 2367–2373.
 12. B. Li and S. Prasad, Basic expressions and approximations in small-signal parameter extraction for HBT's, *IEEE Trans Microwave Theory Tech* 47 (1999), 534–539.
 13. A. Ouslimani, J. Gaubert, H. Hafidallah, A. Birafane, P. Pouvil, and H. Leier, Direct extraction of linear HBT-model parameters using nine analytical expression blocks, *IEEE Trans Microwave Theory Tech* 50 (2002), 218–221.
 14. D. Acosta, W.U. Liu, and J.S. Harris, Jr., Direct extraction of the AlGaAs/GaAs heterojunction bipolar transistor small-signal equivalent circuit, *IEEE Trans Electron Devices* 38 (1991), 2018–2024.
 15. B.L. Ooi, T.S. Zhou, and P.S. Kooi, AlGaAs/GaAs HBT model estimation through the generalized pencil-of-function method, *IEEE Trans Microwave Theory Tech* 49 (2001), 1289–1294.
 16. Y. Gobert, P.J. Tasker, and K.H. Bachem, A physical, yet simple, small-signal equivalent circuit for the heterojunction bipolar transistor, *IEEE Trans Microwave Theory Tech* 45 (1997), 149–153.
 17. F. Herzel and B. Heinemann, High-frequency noise of bipolar devices in consideration of carrier heating and low temperature effects, *Solid-State Electron* 38 (1995), 1905–1909.
 18. S.P. Voinescu, M.C. Maliepaard, J.L. Showell, G.E. Babcock, D. Marchesan, M. Schroter, P. Schvan, and D.L. Hareme, A scalable high-frequency noise model for bipolar transistors with application to optimal transistor sizing for low-noise amplifier design, *IEEE J Solid-State Circuits* 32 (1997), 1430–1438.
 19. G. Niu, W.E. Ansley, S. Zhang, J.D. Cressler, C.S. Webster, and R.A. Groves, Noise parameters optimization of UHV/CVD SiGe HBT's for RF and microwave applications, *IEEE Trans Electron Devices* 46 (1999), 1589–1598.
 20. R.J. Hawkins, Limitations of Nielsen's and related noise equations applied to microwave bipolar transistors, and a new expression for the frequency and current dependent noise figure, *Solid-State Electron* 20 (1977), 191–196.
 21. P. Rouquette, D. Gasquet, T. Holden, and J. Moul, HBT's RF noise parameters determination by means of an efficient method based on noise analysis of linear amplifier networks, *IEEE Trans Microwave Theory Tech* 45 (1997), 690–694.
 22. J.P. Roux, L. Escotte, R. Plana, J. Graffeuil, S.L. Delage, and H. Blanck, Small-signal and noise model extraction technique for heterojunction bipolar transistor at microwave frequencies, *IEEE Trans Microwave Theory Tech* 43 (1995), 293–298.
 23. Q. Cai, J. Gerber, U.L. Rodhe, and T. Daniel, HBT high-frequency modeling and integrated parameter extraction, *IEEE Trans Microwave Theory Tech* 45 (1997), 2493–2502.
 24. A. Lázaro, L. Pradell, and J.M. O'Callaghan, Method for measuring noise parameters of a microwave two-port, *IEE Electron Lett* 34 (1998), 1332–1333.
 25. J. Gao, X. Li, H. Wang, and G. Boeck, Microwave noise modeling for InP-InGaAs HBTs, *IEEE Trans Microwave Theory Tech* 52 (2004), 1264–1272.
 26. J. Gao, X. Li, L. Jia, H. Wang, and G. Boeck, Direct extraction of InP HBT noise parameters based on noise-figure measurements system, *IEEE Trans Microwave Theory Tech* 53 (2005), 330–335.
 27. A. Lázaro, L. Pradell, and J.M. O'Callaghan, FET noise parameter determination using a novel technique based on 50Ω noise-figure measurements, *IEEE Trans Microwave Theory Tech* 47 (1999), 315–324.
 28. M.C. Maya, A. Lázaro, and L. Pradell, Simultaneous extraction of the small-signal equivalent circuit elements and noise parameters of HBTs, *Proc SPIE Int Symp Fluctuations and Noise (FAN-2004) in Devices and Circuits II* 5470 (2004), 429–439.
 29. H. Hillbrand and P. Russer, An efficient method for computer aided noise analysis of linear amplifier networks, *IEEE Trans Microwave Theory Tech* 23 (1976), 235–238.
 30. M. Rudolph, R. Doerner, L. Klapproth, and P. Heymann, An HBT noise model valid up to transit frequency, *IEEE Electron Device Lett* 20 (1999), 24–26.
 31. L. Escotte, J.P. Roux, R. Plana, J. Graffeuil, and A. Gruhle, Noise modeling of microwave heterojunction bipolar transistors, *IEEE Trans Electron Devices* 42 (1995), 883–889.
 32. G.N. Henderson and D. Wu, Noise characteristics of GaAs HBT's, *IEEE MTT-S Dig* (1996), 1221–1224.

© 2006 Wiley Periodicals, Inc.

PHOTONIC-CRYSTAL-FIBER-BASED MACH-ZEHNDER INTERFEROMETER USING LONG-PERIOD GRATINGS

X. Yu, P. Shum, and X. Dong

Network Technology Research Centre
Nanyang Technological University
Research TechnoPlaza, 4th Storey
50 Nanyang Drive, Singapore 637553

Received 4 January 2006

ABSTRACT: We systematically analyze the mode-coupling effects of stress-induced long-period gratings (LPGs) using photonic crystal fiber (PCF). Two Mach-Zehnder interferometers based on this grating are demonstrated. These devices offer the unique advantages of being tunable and reconfigurable. Their good interfering efficiency makes them promising for wavelength-selective filters in WDM communication systems. © 2006 Wiley Periodicals, Inc. *Microwave Opt Technol Lett* 48: 1379–1383, 2006; Published online in Wiley InterScience (www.interscience.wiley.com). DOI 10.1002/mop.21647

Key words: photonic crystal fiber; long period grating; photoelastic effect; Mach-Zehnder interferometer

1. INTRODUCTION

Long-period gratings (LPGs), which satisfy the phase-matching condition between the fundamental core mode and a set of forward-propagating cladding modes in an optical fiber [1–4], are fiber-optic components that are widely used in optical telecommunications and sensors. This grating device has advantages of low back-reflection and insertion loss, insensitivity to electromagnetic interference, and cost-effectiveness. In recent years, many research interests have been attracted to the LPGs in photonic crystal fibers (PCFs) [5–9], which consist of a pure-silica core, and a microstructured air-silica cladding. Because the microstructured cladding consists of air holes, a PCF's cladding index shows strong wavelength dependence. This makes such fibers exhibit some properties that are distinguishable from conventional optical fiber. Inscription of LPGs into such special fibers was demonstrated by periodic stress relaxation using CO₂ laser [6]. However, this tech-